2017 International Symposium on Nonlinear Theory and Its Applications,
NOLTA2017, Cancun, Mexico, December 4-7, 2017

Analysis of bifurcation phenomena of coupled piecewise-constant hysteresis oscillators

Tri Quoc Truong[a], Tadashi Tsubone[b], and Naohiko Inaba[c]

[a] Department of Integrated Bioscience and Technology, Nagaoka University of Technology
Nagaoka, Niigata 940-2188, Japan.
[b] Department of Electrical, Electronics and Information Engineering, Nagaoka University of Technology
Nagaoka, Niigata 940-2188, Japan.
[c] Organization for the Strategic Coordination of Research and Intellectual Properties, Meiji University
Kawasaki, Kanagawa 214-8571, Japan.
Email: qttruong@stn.nagaokaut.ac.jp, tsubone@vos.nagaokaut.ac.jp, naohiko@yomogi.jp

Abstract—This study analyzes the quasiperiodic bifurcation phenomena of two-coupled piecewise-constant hysteresis oscillator driven by a rectangular wave force and three-coupled piecewise-constant hysteresis oscillator. These oscillators can generate three-dimensional tori. By using a generalized calculation algorithm for deriving Jacobian matrices in piecewise-constant hysteresis systems, we conduct two-parameter Lyapunov diagrams for both non-autonomous two-dimensional system and autonomous three-dimensional system. According to the numerical results, Arnol'd resonance web and the hysteresis phenomenon is observed. The hysteresis distorts the Chenciner bubbles in non-autonomous two-dimensional system, however, we cannot observe such phenomenon in the autonomous three-dimensional system.

1. Introduction

In two-dimensional tori-generating systems such as coupled oscillators or forced oscillators, we can observe infinitely many synchronization regions; these regions are well known as Arnol'd tongues. Wherein, periodic solution-generating regions exist in two-dimensional tori-generating regions. However, in three-dimensional tori-generating systems show more complex bifurcation structures. Two-dimensional tori-generating regions exist in three-dimensional tori-generating regions. These partial synchronization regions extend in a numerous of directions like a "cobweb" in dynamics' parameter spaces, which called Arnol'd resonance web. Furthermore, complete synchronization regions of three-dimensional tori are found in two-dimensional tori-generating regions. Such complete synchronization regions and partial synchronization regions were proposed by Linsay and Cumming in Ref [1]. Many researchers have attracted attention to these quasiperiodic bifurcation structures in both discrete-time dynamics [2] and continuous-time dynamics [3, 4].

To analyze bifurcation structures in continuous-time dynamics more precisely, Tsubone et al. proposed and analyzed the fundamental of piecewise-constant hysteresis oscillator driven by a rectangular wave force [5]. Because vector fields of piecewise-constant hysteresis oscillator take only constant values piecewisely, it is relatively easy to perform rigorous analysis. Hence, using the same computational cost similar to that of discrete-time dynamics, Inaba et al. succeed in observing Arnol'd resonance webs with high resolution in a driven piecewise-constant hysteresis oscillators [4]. Subsequently, we analyzed this circuit in detail by deriving Jacobian matrices in a systematic procedure [6].

In this study, we analyze the quasiperiodic bifurcation phenomena in two-coupled piecewise-constant hysteresis oscillator driven by a rectangular wave force and three-coupled piecewise-constant hysteresis oscillator. The calculation algorithm for deriving explicit solutions and the Jacobian matrix in piecewise-constant hysteresis oscillators can be applicable in both these systems. By using this algorithm, the Lyapunov exponents are performed with a precision similar to that of maps. Thus, two-parameter Lyapunov diagrams are easily conducted. The numerical experiments show that Arnol'd resonance web and the hysteresis phenomenon is observed in both non-autonomous system and autonomous system of piecewise-constant hysteresis oscillator. Furthermore, the hysteresis phenomenon erodes the Chenciner bubbles in non-autonomous system.

2. Coupled piecewise-constant hysteresis oscillators

Figure 1(a) presents the fundamental of piecewise-constant hysteresis oscillator without the forcing term that comprises of a capacitor and hysteresis element. The circuit equation is represented by

$$C\frac{\mathrm{d}v}{\mathrm{d}t} = H(v). \tag{1}$$

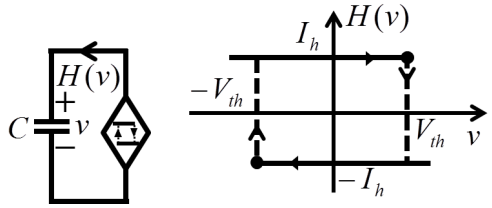

(a) (b)

Figure 1: Piecewise-constant hysteresis oscillator. (a) Circuit diagram. (b) $v-i$ characteristics of the hysteresis element.

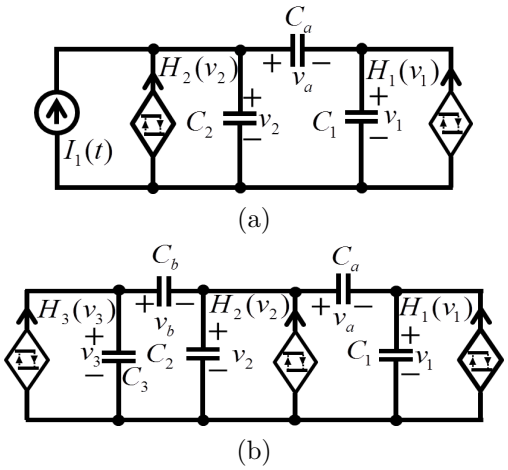

Figure 2: Coupled piecewise-constant hysteresis oscillators. (a) Two-coupled piecewise-constant hysteresis oscillator driven by a rectangular wave. (b) Three-coupled piecewise-constant hysteresis oscillator.

The $v-i$ characteristic of the hysteresis element is shown in Fig. 1(b). If the solution is on the upper branch of $H(v)=I_h$, v is increasing. When it reaches $v=V_{th}$ the solution jumps to the lower branch of $H(v)=-I_h$. In addition, the solution on the lower branch jumps to the upper branch when v decreases and reaches $v=-V_{th}$.

In this study, we consider the two-coupled non-autonomous piecewise-constant hysteresis circuit and three-coupled autonomous piecewise-constant hysteresis circuit as shown in Fig. 2(a) and Fig. 2(b), respectively. The two-coupled non-autonomous circuit comprises two fundamental of piecewise-constant hysteresis oscillators, which are connected by a capacitor C_a, and a rectangular wave current source $I_1(t)$. The voltage across two capacitors C_1 and C_2 are v_1, v_2, respectively. $H_1(v_1)$ and $H_2(v_2)$ are the two hysteresis elements, of which characteristics behave in the same manner in Fig. 1(b). The waveform of the rectangular wave source with amplitude I and period $2T_0$ is shown in Fig. 3. In the similar settings, the three-coupled autonomous circuit comprises three fundamental of piecewise-constant hysteresis oscillators. These three-coupled circuits are connected by two capacitors C_a and C_b. The voltages across three capacitors C_1, C_2, and C_3 are v_1, v_2, and v_3, respectively. $H_1(v_1)$, $H_2(v_2)$, and $H_3(v_3)$ are the three hysteresis elements.

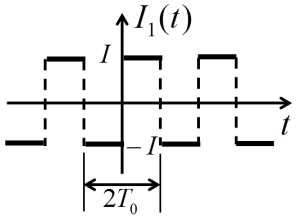

Figure 3: Rectangular wave.

The circuit dynamics of the two-coupled non-autonomous system is described by

$$\begin{aligned}\dot{x}&=k_x=D_3h_1(x)+D_1h_2(y)+S(\tau),\\ \dot{y}&=k_y=D_2h_1(x)+D_2D_4\big(D_1h_2(y)+S(\tau)\big).\end{aligned}\tag{2}$$

where "$\cdot$" denotes the derivative of τ and the following dimensionless variables and parameters are used.

$$\begin{gathered}v_1=V_{th1}x,\ v_2=V_{th2}y,\ t=\gamma\tau,\\ h_1(x)I_{h1}=H_1(V_{th1}x),\ h_2(y)I_{h2}=H_2(V_{th2}y),\\ \gamma=\frac{V_{th1}(C_1C_2+C_1C_a+C_2C_a)}{I_{h1}C_a},\\ \frac{I_{h2}}{I_{h1}}=D_1,\ \frac{V_{th1}}{V_{th2}}=D_2,\ \frac{I}{I_{h1}}=B,\\ \frac{C_2+C_a}{C_a}=D_3,\ \frac{C_1+C_a}{C_a}=D_4,\ \frac{T_0}{\gamma}=T.\end{gathered}\tag{3}$$

The normalized hysteresis loops are $h_1(x)$ and $h_2(y)$. Periodic external force $S(\tau)$ is expressed as follow.

$$S(\tau)=\begin{cases}B \text{ for } nT\le\tau<(n+1)T,\\ -B \text{ for } (n+1)T\le\tau<(n+2)T,\end{cases}\tag{4}$$

where n is integer. B and T is the amplitude and half-periodic of the rectangular wave, respectively. The circuit dynamics include six parameters D_1, D_2, D_3, D_4, B, and T. In the same procedure, the normalized equations for the three-coupled autonomous circuit is represented by

$$\begin{aligned}\dot{x}=k_x=\ &(D_5+D_5D_6-1)h_1(x)+D_1D_6h_2(y)\\ &+D_3h_3(z),\\ \dot{y}=k_y=\ &D_2D_6h_1(x)+D_1D_2D_5D_6h_2(y)\\ &+D_2D_3D_5h_3(z),\\ \dot{z}=k_z=\ &D_4h_1(x)+D_1D_4D_5h_2(y)\\ &+D_3D_4(D_6+D_5D_6-1)h_3(z).\end{aligned}\tag{5}$$

The circuit dynamics include six parameters D_1, D_2, D_3, D_4, D_5, and D_6. Normalized parameters are expressed as follows.

$$\frac{I_{h2}}{I_{h1}} = D_1,\ \frac{V_{th1}}{V_{th2}} = D_2,\ \frac{I_{h3}}{I_{h1}} = D_3,\ \frac{V_{th1}}{V_{th3}} = D_4,\\ \frac{C_a + C}{C_a} = D_5,\ \frac{C_b + C}{C_b} = D_6. \tag{6}$$

3. Derivation of Lyapunov exponents in a piecewise-constant hysteresis oscillator

In this section, we explain the procedure for deriving the Lyapunov exponents by introducing the explicit expression of the solution. To make it easy to conduct rigorous solutions in non-autonomous system, we assume τ in Eq. (2) as a variable. Hence, we can rewrite Eq. (2) in the autonomous form as follows.

$$\begin{aligned} \dot{x} &= k_x = D_3 h(x) + D_1 h(y) + S(\tau), \\ \dot{y} &= k_y = D_2 h(x) + D_2 D_4 \big(D_1 h(y) + S(\tau)\big), \\ \dot{\tau} &= k_z = 1. \end{aligned} \tag{7}$$

We consider the solution where the initial condition at $\tau = \tau_0$ is $\boldsymbol{x_0} = (x_0,\ y_0,\ z_0)^\top$. When the trajectory started at τ_0 hits a boundary line, i.e., either one of $x = \pm 1$, $y = \pm 1$, or $z = \pm 1$ ($\tau = T$ or $\tau = 2T$ in the non-autonomous system's case) at the time τ_1, the solution of Eq. (2) and Eq. (5) is expressed as follows.

$$\boldsymbol{x}_1 = \boldsymbol{x}_0 + \boldsymbol{k}(\tau_1 - \tau_0), \tag{8}$$

where $\boldsymbol{k} = (k_x, k_y, k_z)^\top$ is vector field. To conduct the Jacobian matrix in a systematic manner, a normal vector of the boundary line $\boldsymbol{n}^\top$ is introduced. By using this normal vector, the $(\tau_1 - \tau_0)$ in Eq. (8) is obtained

$$\tau_1 - \tau_0 = \frac{\boldsymbol{n}^\top \boldsymbol{x}_1 - \boldsymbol{n}^\top \boldsymbol{x}_0}{\boldsymbol{n}^\top \boldsymbol{k}}. \tag{9}$$

Note that, at the time τ_1 the trajectory is on the boundary line. If the solution hits the line $x = 1$ the boundary condition is

$$\boldsymbol{n}^\top \boldsymbol{x}_1 = D, \tag{10}$$

where $\boldsymbol{n}^\top = (1, 0, 0)$ and $D = 1$. The other boundary conditions can be expressed similarly and summarized in Table 1. In addition, substituting Eq. (9) into Eq. (8) yields the following equation.

$$\boldsymbol{x}_1 = \left(I_n - \frac{\boldsymbol{k}\boldsymbol{n}^\top}{\boldsymbol{n}^\top \boldsymbol{k}}\right) \boldsymbol{x}_0 + \frac{\boldsymbol{k} D}{\boldsymbol{n}^\top \boldsymbol{k}}, \tag{11}$$

where I_n denotes an identity matrix.

It is clear from Eq. (11) that the local Jacobian matrix A is represented by

$$A = \frac{\mathrm{d}\boldsymbol{x}_1}{\mathrm{d}\boldsymbol{x}_0} = I_n - \frac{\boldsymbol{k}\boldsymbol{n}^\top}{\boldsymbol{n}^\top \boldsymbol{k}}. \tag{12}$$

Table 1: Vector $\boldsymbol{n}^\top$ and values of D.

	$\boldsymbol{n}^\top$	D
$x = 1$	(1 0 0)	1
$x = -1$	(1 0 0)	-1
$y = 1$	(0 1 0)	1
$y = -1$	(0 1 0)	-1
$z = 1$	(0 0 1)	1
$z = -1$	(0 0 1)	-1
$\tau = T$	(0 0 1)	T
$\tau = 2T$	(0 0 1)	$2T$

Then, if the solution hits $x = 1$ or $x = -1$,

$$A_0 = \begin{pmatrix} 0 & 0 & 0 \\ -k_y/k_x & 1 & 0 \\ -k_z/k_x & 0 & 1 \end{pmatrix}, \tag{13}$$

if the solution hits $y = 1$ or $y = -1$,

$$A_1 = \begin{pmatrix} 1 & -k_x/k_y & 0 \\ 0 & 0 & 0 \\ 0 & -k_z/k_y & 1 \end{pmatrix}, \tag{14}$$

and, if the solution hits $z = 1$ or $z = -1$ ($\tau = T$ or $\tau = 2T$ in the non-autonomous system's case),

$$A_2 = \begin{pmatrix} 1 & 0 & -k_x/k_z \\ 0 & 1 & -k_y/k_z \\ 0 & 0 & 0 \end{pmatrix}. \tag{15}$$

Note that the Jacobian matrices A_0, A_1, and A_2 include an all zero row. Therefore, one of eigenvalues of these matrices is zero and the corresponding minimum Lyapunov exponent is $-\infty$.

We use Eq. (11) and (12) to define the first and the second Lyapunov exponent as follows.

$$\begin{aligned} \lambda_1 &\simeq \frac{1}{N} \sum_{j=M+1}^{M+N} \ln \left| A_i^j e_1^j \right|, \\ \lambda_1 + \lambda_2 &\simeq \frac{1}{N} \sum_{j=M+1}^{M+N} \ln \left| A_i^j e_1^j \times A_i^j e_2^j \right|, \end{aligned} \tag{16}$$

where e_1^j and e_2^j are orthonormal bases, and A_i^j is the Jacobian matrix, which is one of A_0, A_1, and A_2. M and N are integers. It is reasonable to argue that for $M = N = 2 \times 10^7$ the two Lyapunov exponents converge to zero. Therefore, Lyapunov exponent is to be regarded as zero if the following equation is satisfied.

$$|\lambda_i| < 1/10^6. \tag{17}$$

4. Arnol'd resonance web and hysteresis phenomenon in coupled piecewise-constant hysteresis oscillators

In this section, we conduct Lyapunov analysis based on Eq. (17). A continuous deformation method is

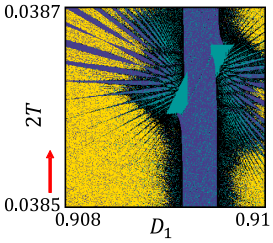

(a)

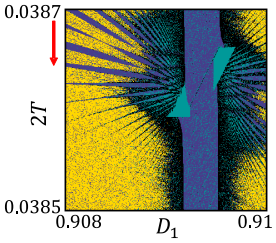

(b)

Figure 4: Lyapunov diagram of the non-autonomous oscillator. (a) Bottom left. (b) Top left. (Parameter values $D_2 = 1.1, D_3 = D_4 = 1001$, and $B = 0.015$).

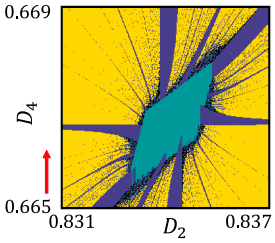

(a)

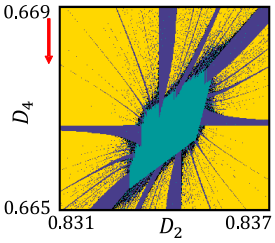

(b)

Figure 5: Lyapunov diagram of the autonomous oscillator. (a) Bottom left. (b) Top left. (Parameter values $D_1 = 1.2, D_3 = 1.5$, and $D_5 = D_6 = 1001$).

used to trace parameter. Fig. 4 and Fig. 5 show two-parameter Lyapunov diagrams. The regions generating the periodic solutions marked in dark cyan. These regions can be denoted as the Chenciner bubbles. Regions generating two-dimensional tori ($\lambda_1 = 0$, and $\lambda_2 < 0$), three-dimensional tori ($\lambda_1 = 0$, and $\lambda_2 = 0$), and chaos are maked in blue, yellow, and black, respectively. The Arnol'd resonance web is clearly observed.

The red arrows show the direction of the tracing parameter in these Lyapunov diagrams. For example, in Fig. 4(a) and Fig. 5(a), we choose initial values at the bottom left and set initial parameter values by varying D_1 (or D_2, respectively) from the bottom left to the bottom right. We trace the parameter $2T$ (or D_4, respectively) from the bottom to the top. In Fig. 4(b) and Fig. 5(b), we trace the parameter $2T$ (or D_4, respectively) from the top to the bottom, with the same manner indicated in Fig. 4(a) and Fig. 5(a). As shown in these figures, the bifurcation structures depend on the initial parameter values, and a hysteresis phenomenon is clearly observed. However, in the non-autonomous circuit's case, the hysteresis erodes the periodic solution-generating regions. This results suggest that the external force significantly affect the bifurcation structures of non-autonomous systems.

5. Conclusion

We discussed the quasiperiodic bifurcation phenomena of coupled piecewise-constant hysteresis oscillators. We used a generalized calculation algorithm for the rigorous solutions in piecewise-constant hysteresis oscillators to conduct Lyapunov analysis for both non-autonomous system and autonomous system. Arnol'd resonance web and the hysteresis phenomenon is observed. The hysteresis distorts the Chenciner bubbles in non-autonomous two-dimensional system. We are interested in whether hysteresis strongly influence on Arnol'd resonance web in higher non-autonomous system, such as three-coupled piecewise-constant hysteresis oscillator driven by a rectangular wave.

References

[1] P. S. Linsay, and A. W. Cumming, "Three-frequency quasiperiodicity, phase locking, and the onset of chaos," *Physica D*, vol.40, pp.196-217, 1989.

[2] M. Sekikawa, N. Inaba, K. Kamiyama, and K. Aihara, "Three-dimensional tori and Arnold tongues," *Chaos*, vol.24, 013137, 2014.

[3] Y. P. Emelianova, A. P. Kuznetsov, L. V. Turukina, I. R. Sataev, and N.Y. Chernyshov, "A structure of the oscillation frequencies parameter space for the system of dissipatively coupled oscillators," *Nonlinear Sci. Numer. simul.*, vol.19, pp.1203-1212, 2013.

[4] N. Inaba, K. Kamiyama, T. Kousaka, and T. Endo, "Numerical and experimental observation of Arnold resonance webs in an electrical circuit," *Physica D*, vol.311-312, pp.17-24, 2015.

[5] T. Tsubone, N. Inaba, T. Tsubouchi, and T. Yoshinaga, "Synchronization phenomena from an extremely simplified piecewise-constant driven oscillator," *IEICE Trans*, vol.J93-A, pp.375-383, 2010 (Japanese).

[6] T. Q. Truong, T. Tsubone, M. Sekikawa, and N. Inaba, "Complicated quasiperiodic oscillations and chaos from driven piecewise-constant circuit: Chenciner bubbles do not necessarily occur via simple phase-locking," *Physica D*, vol.341, pp.1-9, 2017.